Design, simulations, and conditioning of 500 kW fundamental power couplers for a superconducting rf gun

Wencan Xu,[1,*] Z. Altinbas,[1] S. Belomestnykh,[1,2] I. Ben-Zvi,[1,2] M. Cole,[3] S. Deonarine,[1] M. Falletta,[3] J. Jamilkowski,[1] D. Gassner,[1] P. Kankiya,[1] D. Kayran,[1] N. Laloudakis,[1] L. Masi, Jr.,[1] G. McIntyre,[1] D. Pate,[1] D. Philips,[1] T. Seda,[1] T. Schultheiss,[3] A. Steszyn,[1] T. Tallerico,[1] R. Todd,[1] D. Weiss,[1] G. Whitbeck,[3] and A. Zaltsman[1]

[1]*Collider-Accelerator Department, Brookhaven National Lab, Upton, New York 11973, USA*
[2]*Physics & Astronomy Department, Stony Brook University, Stony Brook, New York 11794, USA*
[3]*Advanced Energy Systems, Inc., Medford, New York 11763, USA*
(Received 19 April 2012; published 18 July 2012)

A half-cell superconducting rf electron gun is designed to provide 0.5 A, 2 MeV beam for the Brookhaven National Laboratory R&D Energy Recovery Linac. Total rf power of 1 MW must be delivered to beam to meet the beam current and energy specifications, resulting in very strong coupling. Two opposing fundamental power couplers (FPCs) are employed to minimize the transverse kick to beam traversing the structure and to halve the power through the coupler. A single-window coaxial coupler has been designed to meet the average power and rf coupling requirements. The coupler features a planar beryllia rf window for better handling high thermal stresses and a ''pringle''-shaped tip of the antenna for enhancing rf coupling. Two FPCs have been fabricated and tested in preparation for the gun cryomodule assembly. A room-temperature test stand was used for conditioning couplers in full reflection regime with variable phase of the reflecting wave. The couplers were tested up to 250 kW in pulse mode and 125 kW in cw mode at different settings of the reflecting wave phase to expose all rf surfaces along the couplers to high fields. Several multipacting barriers were encountered and successfully processed away. The rf power levels, at which multipacting was found, match well those found in computer simulations.

DOI: 10.1103/PhysRevSTAB.15.072001 PACS numbers: 29.25.Bx, 29.20.Ej

I. INTRODUCTION

A superconducting rf (SRF) gun photoinjector [1] was chosen to generate high-current, high-brightness electron beam for the Energy Recovery Linac (ERL) at Brookhaven National Laboratory (BNL) [2]. The 704-MHz, half-cell SRF gun requires total rf power of 1 MW in order to meet the beam current and energy specifications (0.5 A, 2 MeV). As a result, very strong rf coupling ($Q_{\text{ext}} = 4 \times 10^4$) between the cavity and transmission line is required. Several coupler options were considered and a coaxial coupler was selected. To enhance coupling, the antenna has a specially shaped tip—an ellipse bent to conform to the profile of the beam pipe—called ''pringle'' [1]. An asymmetric disturbance of the structure's electromagnetic field from a single fundamental power coupler would produce a transverse kick to the passing-by bunches. Because of relatively low energy of the beam, the effect on emittance can be significant. To remedy this, two opposing FPCs are employed with an additional benefit of halving the average power through each coupler (Fig. 1). The coupling scheme is similar to that of the Cornell ERL injector [3], but the coupler design is derived from the fundamental power coupler for Spallation Neutron Source (SNS) superconducting cavities [4]. Table I shows some parameters of the SRF gun and FPC.

The design of SNS couplers was taken as a base line. Several FPC components were then redesigned for better matching at 703.75 MHz and to improve handling of high average power. The rf design, mechanical design, and thermal analysis were done by collaboration of Advanced Energy System, Inc. (AES) and BNL. Two couplers were manufactured for the ERL SRF gun by CPI of Beverly, Massachusetts [5]. To ensure that the FPCs are able to achieve the required power and avoid contamination of the SRF gun, they were cleaned in a particulate-free environment, vacuum baked, and then tested at a conditioning facility prior to installation in the gun. Simulations of multipacting have been carried out with TRACK3P [6] to predict the rf power level and strength of the multipacting zones. Radio-frequency conditioning was performed in the full standing wave regime. Therefore the rf power was limited to 125 kW in cw mode to keep the field at standing wave maximum the same as the field at 500 kW in the traveling wave regime. In

*wxu@bnl.gov

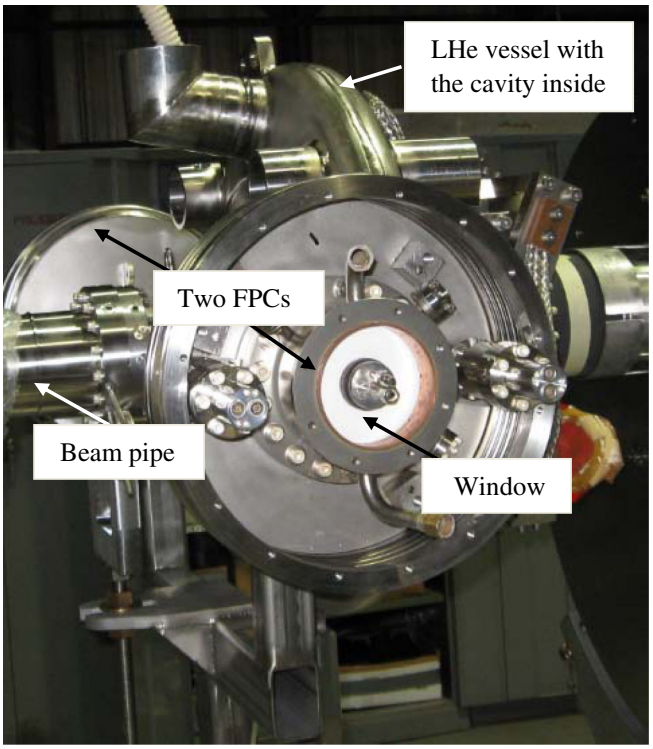

FIG. 1. BNL SRF gun with two opposing FPCs attached.

pulsed mode, the maximum permitted power was 250 kW due to the klystron collector dissipation limit. The conditioning was repeated for different phases of the reflected wave to expose all rf surfaces of the couplers to high fields. Several multipacting barriers were encountered and processed away. The observed multipacting power levels matched well with those predicted by simulations.

In this paper we discuss design of the high power cw fundamental power coupler, multipacting simulations, test, and conditioning of two FPCs, and compare the simulations and test results.

TABLE I. Parameters of the SRF gun and FPC.

Beam energy	2 MeV
Maximum beam current	500 mA
Frequency	703.75 MHz
R/Q	96 Ohm
Q_{ext}	4×10^4
Maximum rf power	1 MW
Maximum rf power per FPC	500 kW
FPC type	Coaxial
Coaxial line impedance	50 Ohm
Number of rf windows per FPC	1
rf window material	Berillia
Coupling type	Antenna

II. FUNDAMENTAL POWER COUPLER DESIGN

Design of the 500-kW fundamental power coupler is derived from the SNS power coupler [4], which in turn is based on the FPC for KEKB SRF cavities [7]. The coaxial-line-based FPC, shown in Fig. 2, is separated by a planar beryllia window into a vacuum side and an air side. On the vacuum side, the copper-plated stainless steel outer conductor is cooled by helium gas and the oxygen-free copper inner conductor has a double-wall design and is cooled by water. Design modifications were implemented to allow for the vacuum side of the coupler, terminated by the rf window, to be within the cryostat envelope. There are no rf-to-water seals. To enhance the coupling between the FPC and the cavity, a pringle-shaped tip (an ellipse bent to conform to the profile of the beam pipe) is attached to the end of the inner conductor.

Berillia, rather than alumina ceramics used in KEKB and SNS couplers, was chosen for rf window fabrication due to its better thermal conductivity and lower dielectric constant. The rf window braze joints are surrounded by rf choke joints to reduce the field. Figure 3 shows the

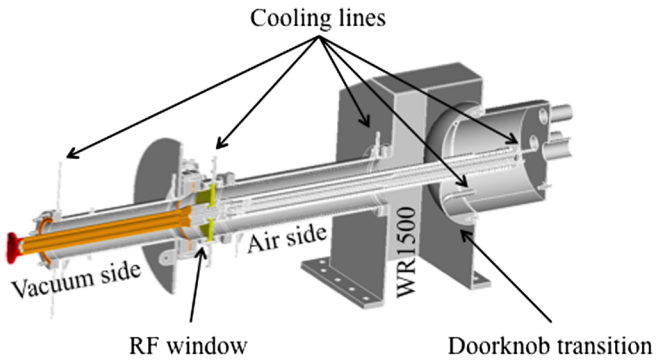

FIG. 2. Fundamental power coupler for the BNL SRF gun.

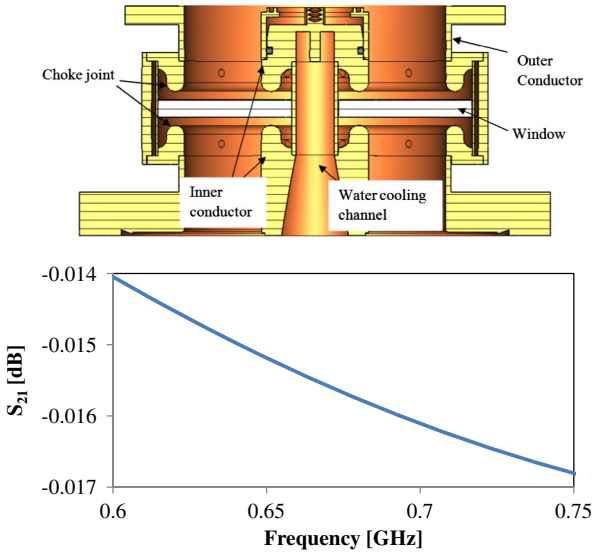

FIG. 3. Top: the planar rf window assembly; bottom: S21 parameter of the rf window.

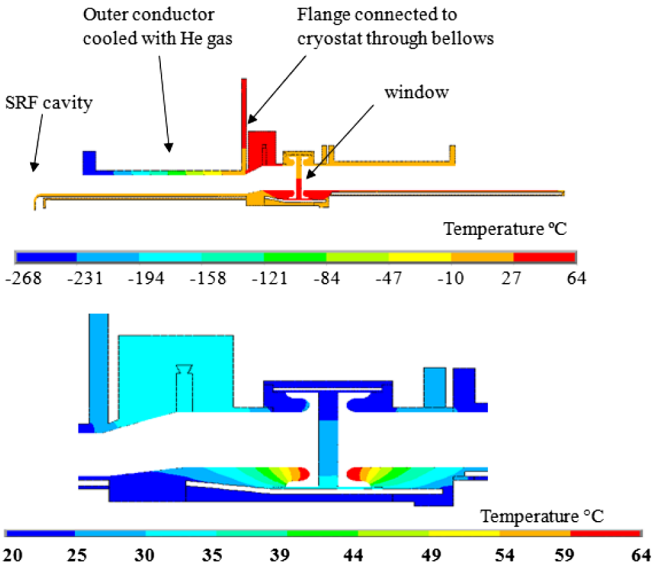

FIG. 4. Top: temperature of the FPC with 1 MW of rf power transmitted through; bottom: temperature contours on the rf window area.

assembly of the rf window and its rf performance. Thermal and mechanical stress analyses were performed for the window under 1 MW rf power using the 3D code ANSYS [8]. Figures 4 and 5 show temperature and stress contours in the window area with 1 MW rf power through (no reflections). The maximum temperature, 61°C, in the window area is at the inner choke. The maximum stress at the window is 6144 psi or 42.4 MPa from the heat load and ambient pressure, which is approximately one third of the

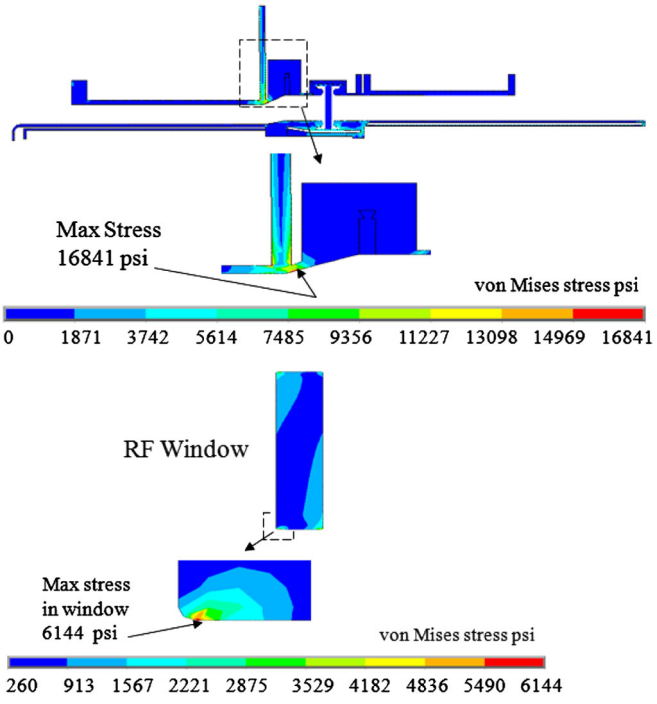

FIG. 5. Von Mises stress contours under 1 MW of rf power.

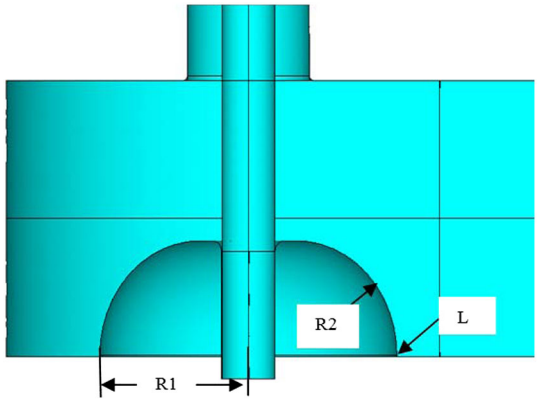

FIG. 6. Doorknob geometry and optimization parameters.

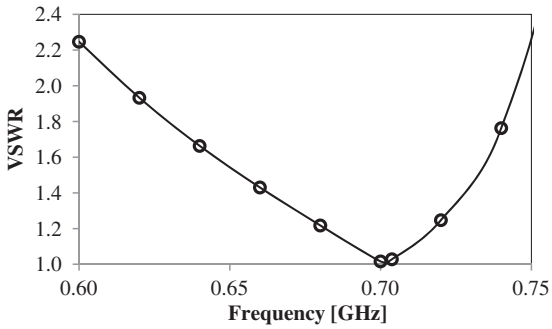

FIG. 7. Calculated VSWR of the doorknob.

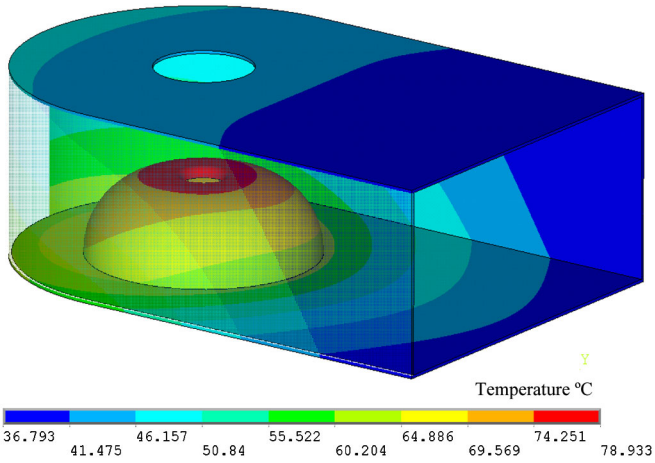

FIG. 8. Temperature contours for the 1 MW rf power.

tensile strength of BeO. At 500 kW rf through power, the maximum temperature at the choke is 41°C and the maximum stress at the window is 3300 psi or 22.7 MPa. The cooling water temperature rise will be less than 0.1°C with 6.9 GPM or 0.44 l/s flow rate around the outer diameter of the window (entering at 20°C). The planar ceramic window assembly has five instrumentation ports on the vacuum side: two for vacuum gauges, two for arc detectors,

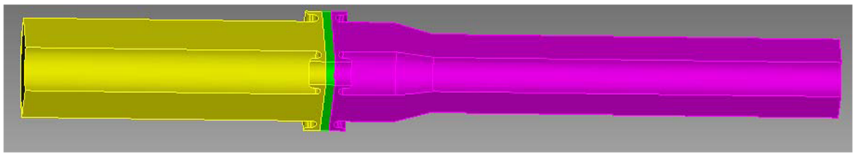

FIG. 9. FPC model for multipacting simulations: magenta—vacuum side; green—window; yellow—air side.

and one spare. The helium gas cools the vacuum side outer conductor through counter flowing helium gas from the cold flange with 5 K helium gas inlet to the bottom of the rf window with 300 K outlet. The flow rate for the helium gas is 0.075 g/s. The total heat load of the two fundamental power couplers is less than 7 W.

On the air side, both the copper-plated stainless steel outer conductor and copper inner conductor are water cooled with a double-wall design. The transition between the coaxial line of the FPCs and WR1500 waveguide has a doorknob configuration. In order to obtain a minimal voltage standing wave ratio, we optimized dimensions of the doorknob shown in Fig. 6: the straight length (L), the seat radius (R1), and the head radius (R2). Figure 7 shows the doorknob VSWR after optimization. The three parameters were also varied to assess the design tolerances. The tolerance analysis shows that the VSWR remains below 1.1 with ± 0.4 mm change of each parameter. The thermal analysis was carried out for the waveguide transition and doorknob under heat load from 1 MW rf power transmitted through. Figure 8 shows the temperature contours in the waveguide transition and doorknob. The waveguide temperature at the head of the doorknob was calculated to be 74°C. To keep the temperature rise reasonable (<1°C) under 1 MW through (no reflection), the doorknob requires cooling by a water flow of 1 GPM (or 0.063 l/s) along the inner corner of the doorknob.

III. SIMULATIONS OF MULTIPACTING

Simulations of multipacting in the FPC were carried out using TRACK3P [6], a 3D particle tracking code. Figure 9 shows the side view of the FPC model used in simulations. The input power was swept from 1 to 250 kW with full reflection at different phases of reflection, which later allowed us to compare the simulation results directly with the actual FPC conditioning in a standing wave mode. At each power level, 50 or more rf cycles were simulated to obtain parameters of the resonant trajectories. A secondary emission yield (SEY) curve for oxygen-free copper after 200°C bake used in simulations is shown in Fig. 10. Multipacting is possible if the final impact energy of the electrons after 50 rf cycles is in the region from 120 to 2500 eV, where SEY > 1.

TRACK3P determines the input power by using the S parameters calculated by S3P, which belongs to the same ACE3P suite of codes developed at SLAC [8]. With the calculated S parameters, the TRACK3P can easily scale

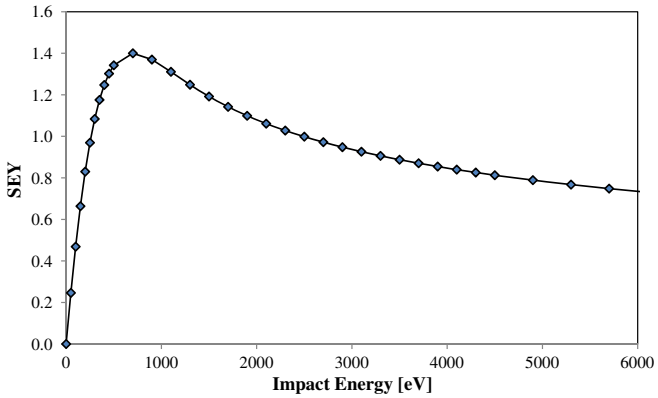

FIG. 10. Secondary emission yield curve for copper used in multipacting simulations.

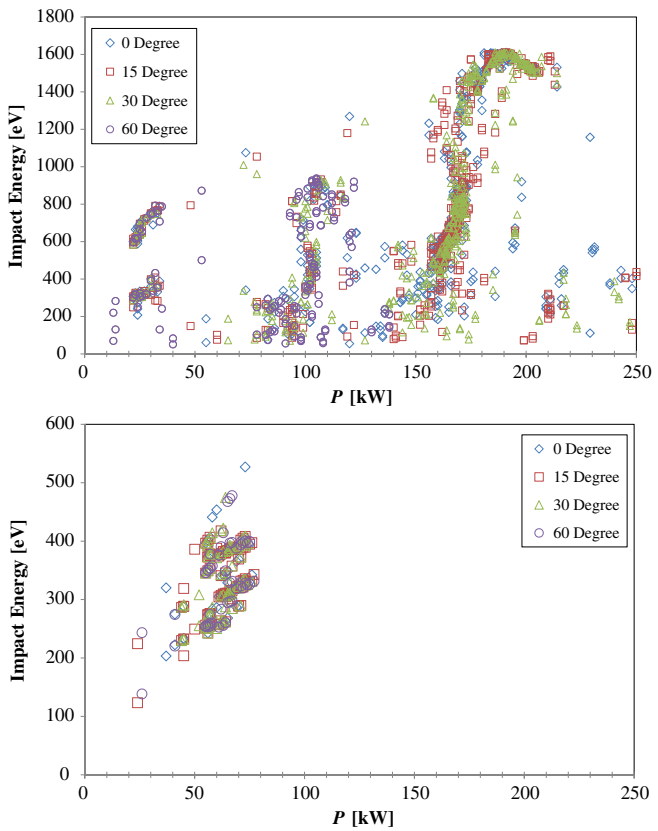

FIG. 11. Multipacting in the coupler at different reflection phases: top plot—vacuum side coaxial line; bottom plot—window.

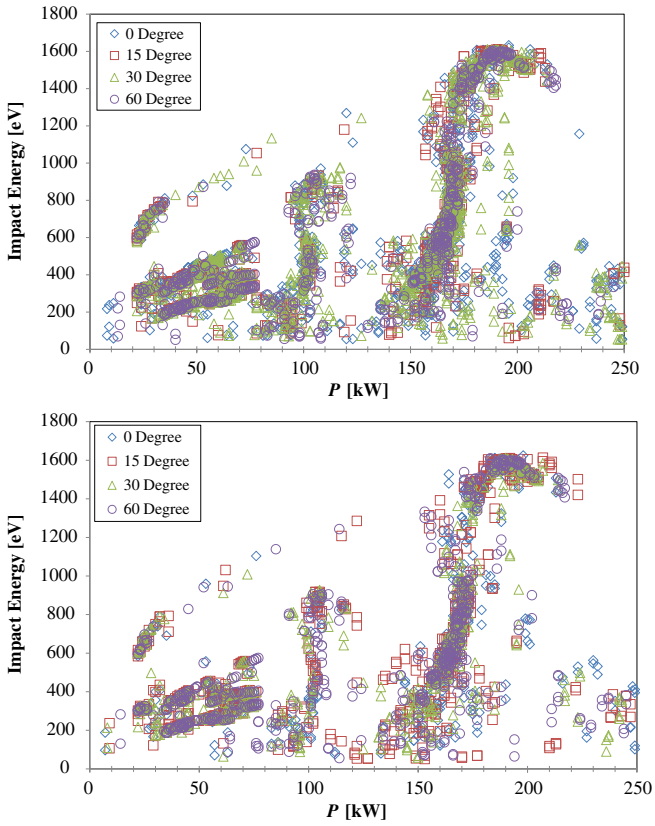

FIG. 12. Multipacting simulation at different frequencies: top plot—703.9 MHz; bottom plot—703.75 MHz.

fields to any power level. The simulation results show (Fig. 11) that multipacting occurs mostly in the vacuum side coaxial line. Multipacting in the rf window area was found only between 24 and 77 kW. Additionally, the multipacting zones are not sensitive to the rf phase of the reflected wave. Plots in Fig. 11 indicate strong multipacting at rf power levels of about 22 to 35 kW, 40 to 77 kW (window), 78 to 120 kW, and about 135 to 205 kW. The simulations also show that multipacting zones are

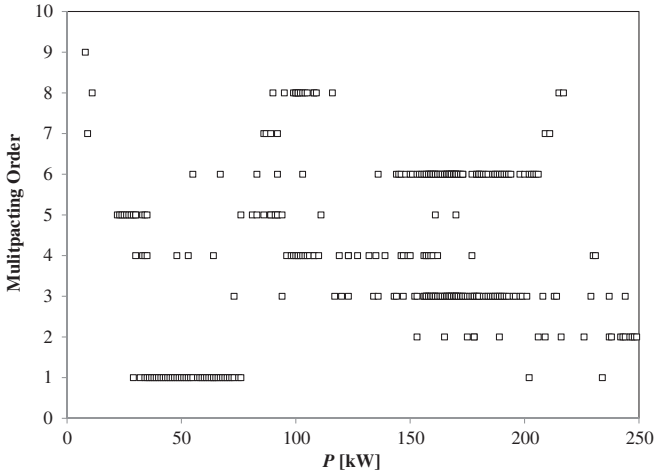

FIG. 14. Multipacting order at different rf power levels.

not sensitive to the rf frequency (Fig. 12). However, the strength of multipacting varies with the frequency change. The simulations show that the dominant is the two-surface multipacting. Figure 13 shows typical multipacting trajectories: in the coaxial line (left picture), which is a two-surface multipacting, and between the window and the choke (right picture). The order of multipacting at different rf power levels is shown in Fig. 14.

IV. FPC CONDITIONING SETUP

A. FPC conditioning stand

The FPC conditioning stand, shown in Fig. 15, is assembled on a robust, mobile aluminum cart [9]. It consists of a vacuum pump system and connecting waveguide. Radio-frequency conditioning of the couplers is performed under ultrahigh vacuum (UHV). UHV is maintained by a turbomolecular pump, which is backed by a dry (oil-free) mechanical pump. The vacuum near the ceramic window is measured with two magnetron gauges, providing vacuum signals for rf power level controls during the conditioning.

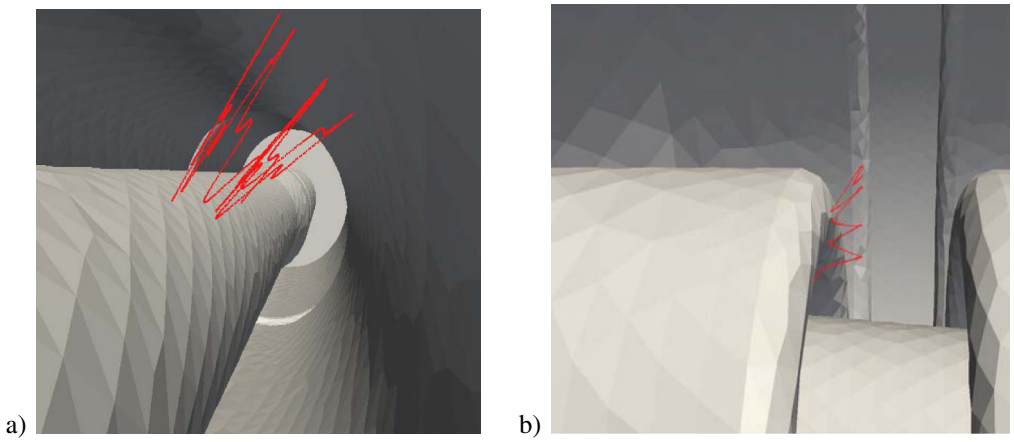

FIG. 13. Multipacting at 110 kW in the coaxial line (a) and between the window and choke at 60 kW (b).

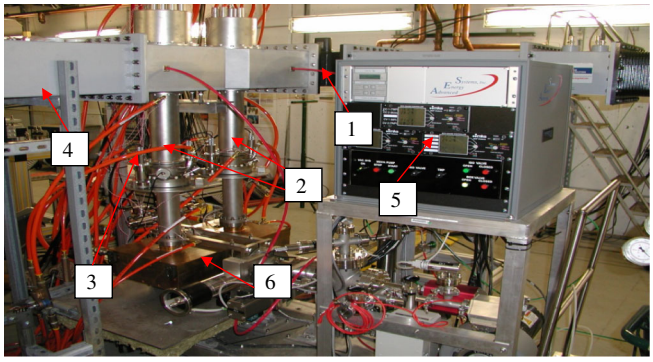

FIG. 15. Assembly of the FPCs for conditioning: 1—waveguide connecting to 1 MW klystron; 2—two FPCs; 3—cooling hoses; 4—waveguide phase shifter and a short plate; 5—vacuum instrument on the conditioning cart; 6—connecting waveguide.

In addition, a residual gas analyzer is provided for leak checking. A fast-response vacuum controller provides signal to the machine protection system (MPS) to shut down rf if vacuum becomes poor. Two FPCs are mounted on the connecting waveguide to be conditioned simultaneously.

B. Assembly

The FPC conditioning cart and FPCs were assembled at AES, which fabricated the conditioning cart. All components (bellows, vacuum manifolds, connecting waveguide) were cleaned by immersion in an ultrasonic bath and dried with dust-free nitrogen gas before assembly. Prior to drying, the window assemblies were also rinsed with deionized water to reduce concentration of dust particles and contaminants trapped on the window. The assembly of vacuum components was carried out in a class 100 clean room. The entire assembly was checked for vacuum leaks. Finally, the conditioning cart was delivered to BNL.

At BNL the cart vacuum system was baked out at 200°C using a thermal-insulation box. It took 7 hours to ramp the temperature up to 200°C (measured at rf window). The stand was kept at this temperature for 20 hours, then the temperature was ramped down at a rate of 15°C/hr. The vacuum reached 7.3×10^{-9} Torr immediately after baking and dropped to 3×10^{-9} Torr after several days of pumping. A vacuum leak check was performed after the bake to ensure that the system is still leak tight. Then the air sides of the FPCs, including the inner and outer conductors and waveguide doorknob transitions, were assembled. S parameter measurements were carried out with two adapters connecting to the doorknob waveguide. Finally, the FPCs were connected to the rf system.

C. rf system

The conditioning was carried out in a standing wave mode. One FPC is connected to a circulator downstream of a 1 MW cw klystron [10], the other one is connected to a variable rf phase shifter and a short plate. Four sets of

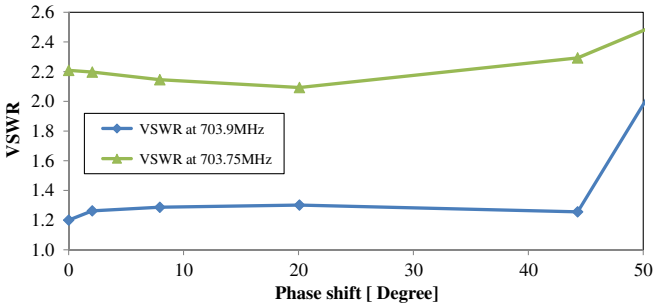

FIG. 16. VSWR measurements of the FPC test setup.

directional couplers (one before the circulator, one before the water load, one before and one after the FPC cart) are used to measure rf power levels. The MPS permission sums arc detector, vacuum, and water flow signals to enable the klystron operation. Prior to conditioning, two waveguide adapters were connected to the upstream and downstream of the couplers, and S parameters were measured for different settings of the phase shifter. Minimum VSWR was measured at 703.9 MHz. In Fig. 16, we compare VSWR at 703.75 and 703.9 MHz. The main reason for relatively big reflection is nonideal matching of the connecting waveguide. The phase shifter has a useful range of only 45 degrees, although its total range is 90 degrees. This explains increase of VSWR at the end of the range in Fig. 16. The -1 dB bandwidth of the klystron is larger than -0.7 MHz with the central frequency at 703.75 MHz. This allowed us to condition the coupler at 703.9 MHz.

V. FPC CONDITIONING RESULTS AND COMPARISON WITH SIMULATIONS

The FPC conditioning began in various pulse modes, from 100 μs/10 ms to 2 ms/10 ms pulse length/period, followed by cw mode with gradual increase of rf power to the maximum value. The rf phase of reflected wave was varied from 0 to 45 degrees from the ERL control room via a remote motor control of the phase shifter.

The output of the klystron was controlled by a computer program with feedback on vacuum. The rf power was automatically increased or decreased depending on vacuum level at the two rf windows relative to three set points according to the following algorithm. If the vacuum was worse than set point 2, but better than set point 3, the amplitude was kept constant. If the vacuum was worse than set point 3, the amplitude was reduced at a preset rate. Unless the vacuum was better than set point 1, the rf amplitude was not increased again.

During the test, we encountered and conditioned multipacting zones at 8 to 10 kW, 16 to 25 kW, 40 to 70 kW, 85 to 120 kW, and about 165 to 185 kW. Above 185 kW, there was a lot of outgassing. Figure 17 shows typical rf and vacuum behavior during conditioning of two zones. The figure shows vacuum bursts at times when the rf power is zero. The sample rate was 200 Hz for vacuum signal and

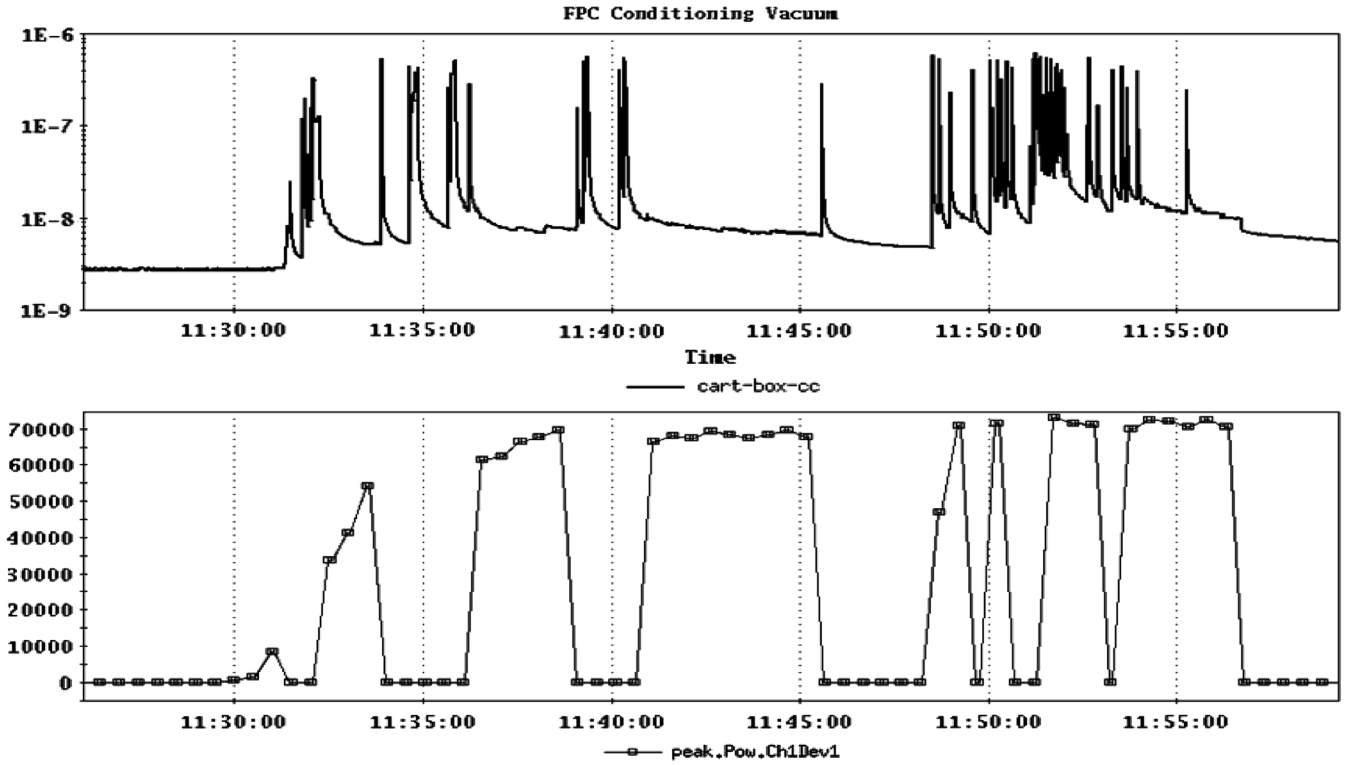

(a) MP processing from about 40 to 70 kW: top plot – vacuum in Torr; bottom plot – RF power in watt.

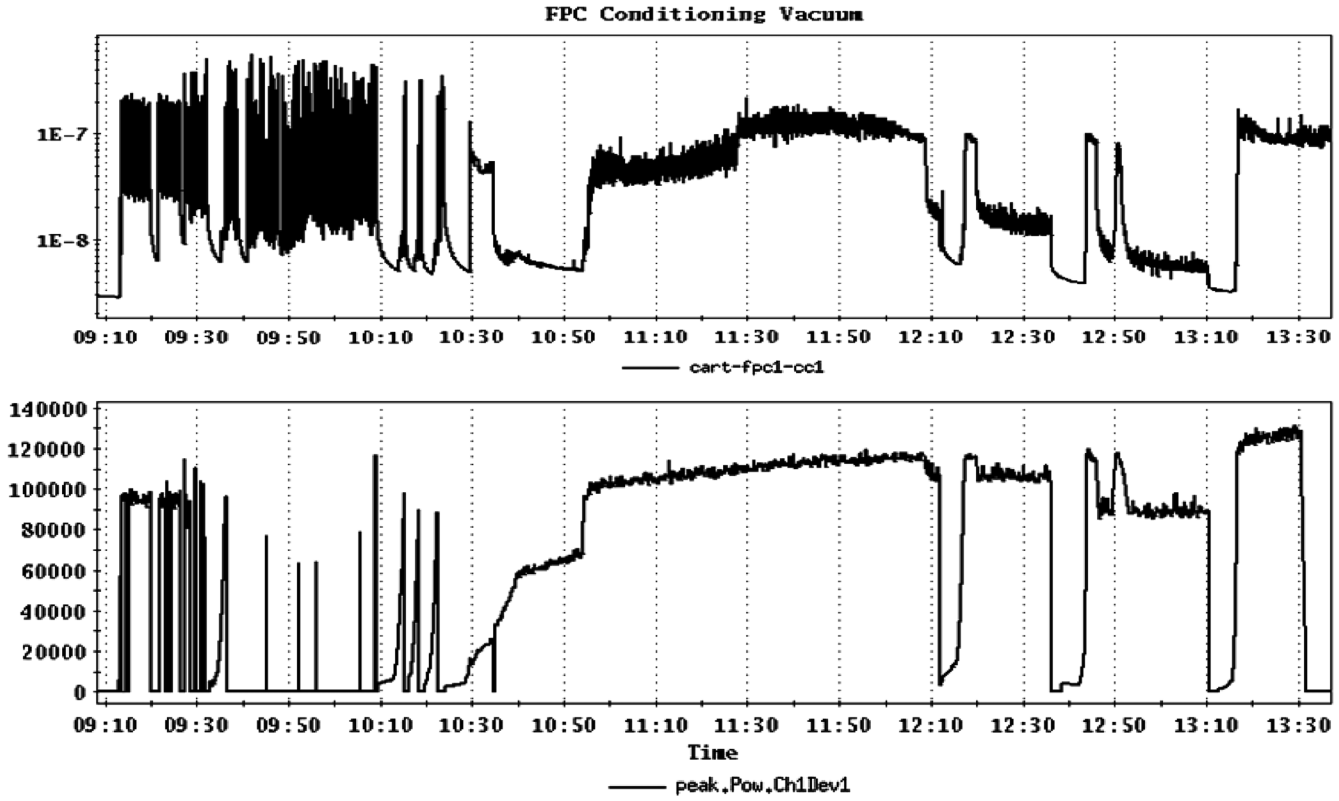

(b) MP processing from about 90 to 120 kW: top plot – vacuum in Torr; bottom plot – RF power in watt.

FIG. 17. Typical rf power and vacuum signals during FPC conditioning.

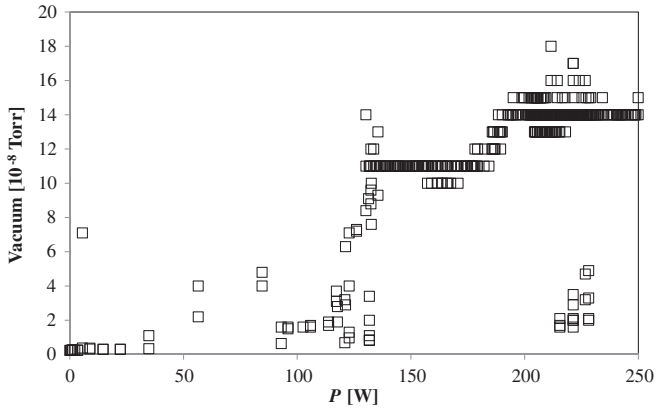

FIG. 18. FPC vacuum vs rf power.

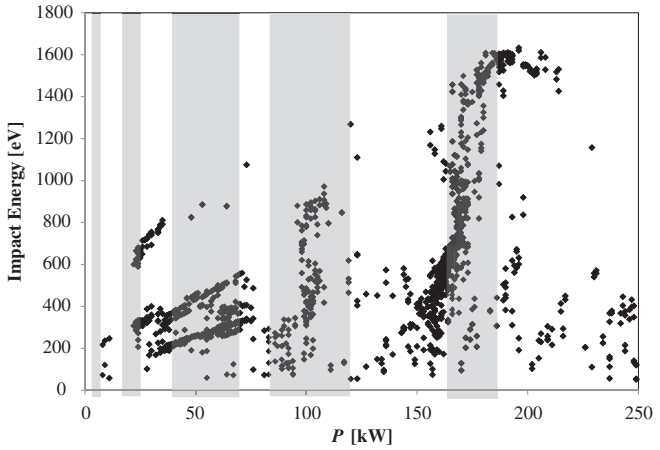

FIG. 19. Comparison of multipacting zones from FPC conditioning test (grey-shaded areas) and simulation results at 703.9 MHz with 0° (black dots).

0.1 Hz for rf power signal. Thus, if the vacuum rises rapidly after rf turn-on, triggering MPS, it is very likely that the data acquisition system would miss short rf pulse and indicate zero rf power as it is evident from the plots. Figure 18 shows typical vacuum during FPC conditioning from 0 to 250 kW. For different rf phases, the processing went similarly and the conditioning time was close except for the very first run, which took most of the test time to ramp-up the rf power and it was a much shorter time for the later runs.

Simulations and test results match reasonably well as is evident from Fig. 19. Shaded areas indicate observed multipacting zones, which are 8 to 10 kW, 16 to 25 kW, 40 to 70 kW, 85 to 120 kW, and about 165 to 185 kW. After FPCs were conditioned at 0° of rf phase, the procedure was repeated at every 10 degrees by adjusting the phase shifter. No multipacting zones other than those shown in Fig. 19 were found. It confirmed nonsensitivity of the multipacting power levels to the phase of reflection, as multipacting mainly occurs in the coaxial line, and only one multipacting zone happened at the window.

V. CONCLUSIONS

To satisfy requirements of the SRF gun for R&D ERL, we designed a high power cw fundamental power coupler capable of delivering up to 1 MW of rf power in the traveling wave, twice as high as required for the gun operation. Two FPCs were fabricated and conditioned using a room-temperature test set up in standing wave mode at different phases of reflected wave. Prior to the conditioning, simulations of multipacting were carried out with TRACK3P, predicting several multipacting barriers. Only one of the barriers was found at the rf window location, the rest were in the coaxial line. A 1 MW klystron was used for conditioning in pulsed and cw regimes. In the pulsed regime the rf power was limited to 250 kW due to the klystron collector dissipation limit. Radio-frequency power in cw mode was limited to 125 kW, which generates field at standing wave maximum the same as the field at 500 kW in traveling wave. The rf power levels, where multipacting was found and processed during rf conditioning of FPCs, agreed reasonably well with multipacting zones predicted by computer simulations. The fundamental power couplers were successfully tested to desired rf power levels and are now installed into the SRF gun cryomodule for operation with beam.

ACKNOWLEDGMENTS

This work is supported by Brookhaven Science Associates, LLC under Contract No. DE-AC02-98CH10886 with the U.S. DOE. The authors would like to acknowledge Lixin Ge, Lining Xiao, Kwok Ko, and Ng Cho of SLAC for help with the TRACK3P simulations. The authors would like to thank Eric Montesinos from CERN for helpful discussions.

[1] R. Calaga *et al.*, Physica (Amsterdam) **441C**, 159 (2006).
[2] D. Kayran *et al.*, in *Proceedings of the 2011 Particle Accelerator Conference, NY, USA* (IEEE, New York, 2011), pp. 2148–2150.
[3] V. Shemelin, H. Padamsee, and S. Belomestnykh, Cornell LEPP Report No. ERL 03-04, 2003.
[4] K. M. Wilson *et al.*, in Proceedings of the 10th Workshop on RF Superconductivity, Tsukuba, Japan, 2001, pp. 535–539 [http://accelconf.web.cern.ch/accelconf/srf01/papers/pt021.pdf].
[5] CPI, http://www.cpii.com/division.cfm/8.
[6] Z. Li *et al.*, in *Proceedings of the 2007 Particle Accelerator Conference, Albuquerque, New Mexico* (IEEE, New York, 2007), pp. 889–893.
[7] S. Mitsunobu *et al.*, in Proceedings of the 1999 Workshop on RF Superconductivity, Santa Fe, NM, USA, pp. 505–507 [http://accelconf.web.cern.ch/accelconf/SRF99/papers/wep032.pdf].
[8] ANSYS, http://www.ansys.com/.
[9] Wencan Xu *et al.*, in Proceedings of the 2011 Particle Accelerator Conference, NY, USA (Ref. [2]).
[10] S. J. Lenci *et al.*, Report No. BNL-82365-2009-CP.